August 27-31, 2023
FLORENCE - ITALY
ICWE 16
16th International Conference on Wind Engineering

Instability mode in flow fields around rectangular prisms

Zhanbiao Zhang [1], Ahsan Kareem [2], Fuyou Xu [3]

[1]*Dalian University of Technology, Dalian, China, zhanbiao@dlut.edu.cn*
[2]*University of Notre Dame, Notre Dame, USA, kareem@nd.edu*
[3]*Dalian University of Technology, Dalian, China, fuyouxu@dlut.edu.cn*

SUMMARY:
Large-eddy simulations of the unsteady flows around rectangular prisms with chord-to-depth ratios (*B*/*D*) ranging from 3 to 12 are carried out at a Reynolds number of 1000. A particular focus of the study is the physical mechanisms governing the global instability of the flow. Based on the dynamic mode decomposition, the interactions between the leading- and trailing-edge vortices at different *B*/*D* values are revealed. It is found that the phase difference between the leading- and trailing-edge vortices is the critical factor promoting a stepwise increase in the Strouhal number with increasing *B*/*D*. According to the phase analysis, there are two types of pressure feedback-loop mechanisms maintaining the self-sustained oscillations. Self-sustained oscillations of the shear layer still exist after a splitter plate is placed in the near wake, indicating that the trailing-edge vortex shedding is not essential in triggering the global instability. Nevertheless, with the participation of the trailing-edge vortex, the primary instability mode may be re-selected due to the upper and lower limits of the shedding frequency imposed by the trailing-edge vortex.

Keywords: rectangular prism, vortex shedding, Strouhal number

1. INTRODUCTION

Flow around a flat rectangular prism is characterized by massive flow separation at the sharp leading edges, unsteady flow reattachment on the afterbody, and trailing-edge Karman-type vortex shedding. Nakamura et al. (1991) found that the Strouhal number (*St*) based on the prism width and free-stream velocity increase stepwise against the chord-to-depth ratio (*B*/*D*) within *B*/*D* = 3~12. They attributed the formation of the large-scale vortices to the impingement of the separated shear layers on the sharp trailing-edge corners and thus called the mechanism the impinging shear-layer (ISL) instability. Later, Naudascher & Rockwell (1994) called the global instability the impinging leading-edge vortex (ILEV) instability to emphasize that it is the large-scale vortices shed from the leading-edge shear layer that interacts with the trailing edge rather than the shear layer itself. Hourigan et al. (2001) noted that the trailing-edge vortex shedding (TEVS) played an important role in the self-sustained oscillations and was responsible for the stepwise progression of the Strouhal number with *B*/*D*.

Although it is widely accepted that the flow around a rectangular prism is governed by the ISL or ILEV instabilities, sometimes accompanied by TEVS, there remain some significant questions to be answered. For example, the complex interaction behaviour between the ILEV and TEVS, the exact form of the pressure feedback loop controlling the global instability for different *B*/*D*, the

range and source of the preferred shedding frequency of TEVS, and the underlying mechanisms of the mode switches at certain *B*/*D* values and the stepwise increase manner of St have not been fully explored.

In the present study, the large-eddy simulation method and the dynamic mode decomposition (DMD) technique are used to extract coherent structures in the ILEV and TEVS and to uncover the pressure feedback-loop mechanism of the global instability and the fundamental mechanism for the stepwise variation of *St* with *B*/*D*. Two special cases are included to explore the roles played by the TEVS in the self-sustained oscillations of the shear layers by separating the ILEV and TEVS.

2. NUMERICAL MODEL

Figure 1 shows the prism geometry, computational domain, and boundary conditions for three-dimensional large-eddy simulations. First, rectangular prisms with *B*/*D* values ranging from 3 to 12, with a unit interval, are used to investigate the variations of the flow characteristics with *B*/*D*. Furthermore, two special configurations are presented to separate the ILEV and TEVS. Case II is characterized by a splitter plate in the wake to eliminate the TEVS. In Case III, the leading-edge separated shear layer is removed, and only TEVS is expected to occur.

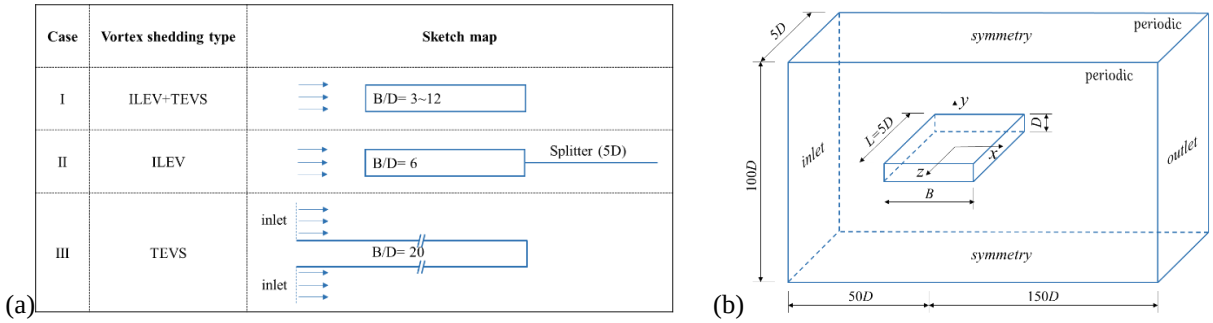

Figure 1. Computational model: (a) prism geometry and (b) computational domain and boundary conditions

The mesh in the *x*-*y* plane is hybrid, with 20 layers of structured grids around the prism and unstructured quadrilateral grids in the rest of the domain. The grid size within the structured region is 0.02D×0.02D, leading to a unit grid aspect ratio and an average y^+ about 1.0 and a maximum y^+ about 3.0 during simulations. The three-dimensional mesh is obtained by extruding the two-dimensional mesh along the spanwise direction with a uniform step size (0.05*D*). The total cell number for regular prisms varies from 9.6 to 15.1 million.

3. RESULTS AND ANALYSIS

3.1. Flow Characteristics for *B*/*D* = 5

To reveal the interactions between the ILEV and TEVS, the evolution of vortex structures during one vortex shedding period in the original flow and the *St* mode are shown in Fig. 2. The *St* mode has a single oscillating frequency of 0.571 and is extracted based on the DMD technique. It is worth emphasizing that the L vortex shedding in the original flow is equivalent to the

alternative shedding of the counter-rotating vortex pairs in the *St* mode.

The ILEV, TEVS, and their interaction process are recognized through the DMD mode. The first half cycle of the *St* mode corresponds to the complete shedding and interaction of *L*1 and *T*1. The evolution in the second half cycle is similar to that of the first half cycle, except that the rotation direction of the shed vortices (*L*2 and *T*2) is opposite to the first half cycle. This shedding and merging behaviours of the *L* and *T* vortices at the trailing edge provide direct supporting evidence for the vortex interaction hypothesis suggested by Hourigan et al. (1993).

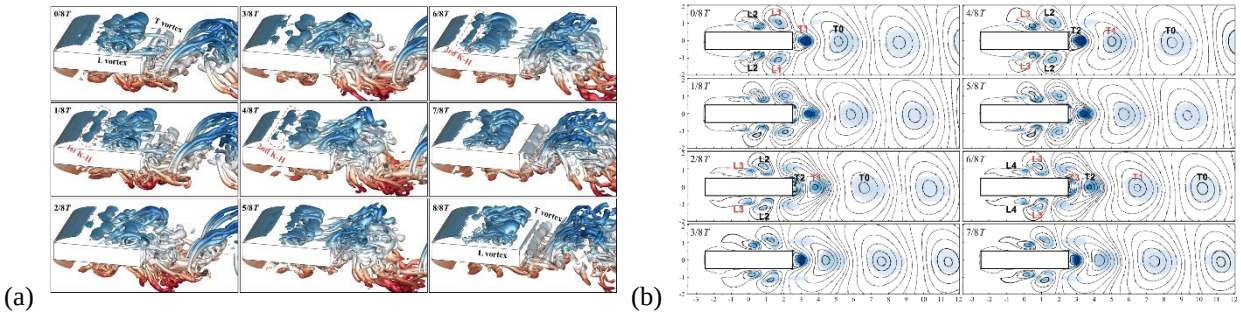

Figure 2. Evolution of the vortical structures in (a) the original flows and (b) the DMD mode for *B*/*D* = 5.

3.2. Effect of B/D on Flow Characteristics

The *St* calculated from the spectra of the lift coefficient is plotted in Fig. 3(a). The predominant frequency component (referred to as the main *St* mode below) at a specific *B*/*D* is marked by a solid circle, while the other frequencies are marked by empty circles. The simulation results show good agreement with the existing results. The stepwise increasing behaviour of the main *St* with *B*/*D* is captured. Mode 1 to Mode 5 represent the five *St* modes as the *St* value increases from 0.6 to 3.0, with a step size of 0.6.

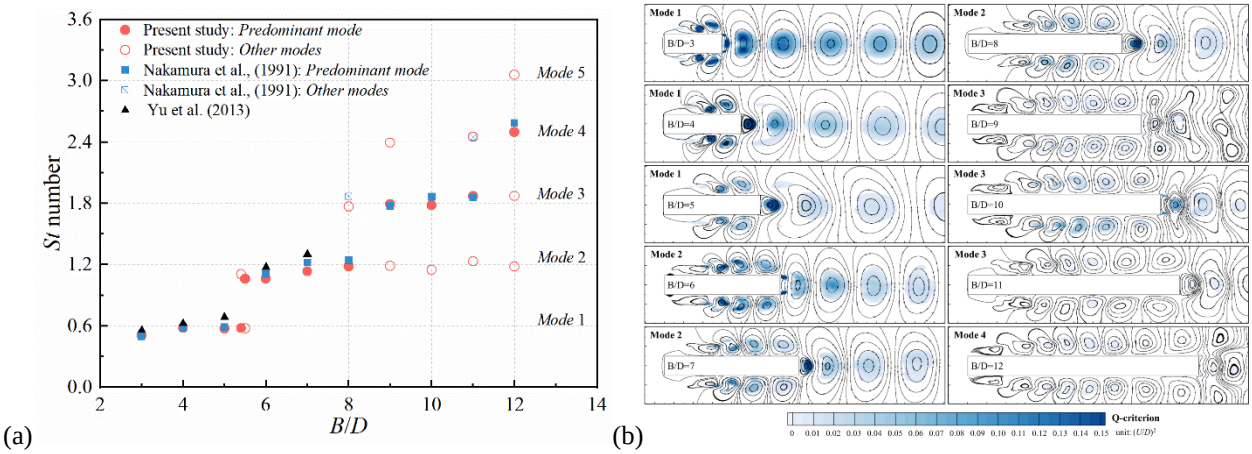

Figure 3. Variations of (a) *St* number and (b) *St* mode with *B*/*D*.

The main *St* mode at each *B*/*D* is extracted from the spanwise-averaged velocity field, as shown in Fig. 3(b). For *B*/*D* = 3−5, 6−8, 9−11, and 12, there are one, two, three, and four pairs of *L* vortices on each side of the prism, respectively. Within each mode, the phase difference between the TEVS and ILEV at the trailing edge increases with *B*/*D* until it reaches π, thus promoting the

transition from the lower mode to the higher mode.

3.3. Flow Characteristics for Cases II and III

The *St* number for Case II is 1.776, corresponding to Mode 3 ($St \approx 0.18$) in Fig. 3(a). The corresponding DMD mode is extracted from the spanwise-averaged velocity field, as shown in Fig. 4(a). The TEVS is eliminated by the splitter plate, but the regular ILEV is still evident, indicating that TEVS is not a necessity for the global instability. However, the participation of TEVS may significantly influence the frequency and intensity of global instability.

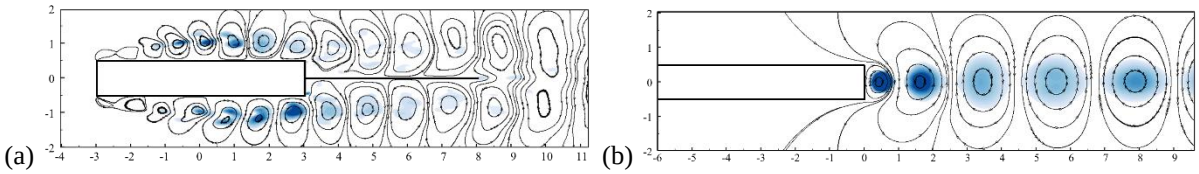

Figure 4. *St* modes for (a) Case II and (b) Case III.

Since the prism width in Case III has no direct meaning, the *St* is calculated based on *D* and is 0.195. If the *St* number of the regular rectangular prisms (Case I) is calculated based on *D*, it is found that the *St*(*D*) experiences a monotonic decrease with *B/D* within each mode, but shows a sudden increase around the mode jump. However, the *St*(*D*) is always distributed within the range of 0.11−0.21. The upper limit is close to the *St* of Case III where only TEVS exists. The lower limit is achieved by the interference effect of TEVS on ILEV though their phase difference. Due to the above limitations imposed by the TEVS, only the most suitable modes, whose frequencies fall into the preferred range of TEVS, will be selected and enhanced by the system for each *B/D*. It is worth mentioning that the TEVS decides which instability mode should be selected, but it does not directly change the frequency of a specific mode. The mode frequency is governed by the pressure feedback-loop mechanism and is characterized by an integral multiple of 0.6 (based on *B*).

4. CONCLUSIONS

The leading- and trailing-edge vortices merge together in the near wake, and the level of development of trailing-edge vortices is dependent on *B*/*D*. Due to the interaction between the ILEV and TEVS, only the most suitable ILEV modes whose frequencies fall into the preferred range of TEVS will be selected and enhanced by the system for each *B/D*, leading to the stepwise increase in *St* with *B*/*D*.

ACKNOWLEDGEMENTS

This work was financially supported by the National Science Foundation of China (grant number 52208464) and the China Postdoctoral Science Foundation (grant number 2022M710589).

REFERENCES

Nakamura, Y., Ohya, Y., & Tsuruta, H. (1991). Experiments on vortex shedding from flat plates with square leading and trailing edges. Journal of Fluid Mechanics, 222, 437–447.

Naudascher, E. & Rockwell, D. (1994). Flow-Induced Vibrations: An Engineering Guide. AA Balkema, Rotterdam, Holland.

Hourigan, K., Thompson, M. C., & Tan, B. T. (2001). Self-sustained oscillations in flows around long blunt plates. Journal of Fluids and Structures, 15(3−4), 387–398.